Proceedings of the 20th International Conference on Soil Mechanics and Geotechnical Engineering– Rahman and Jaksa (Eds)

Bearing capacity of caisson foundations under combined loading

Capacité portante des fondations sur caissons sous chargement combinés

Alessandra Rosati & Sebastiano Rampello
Department of Structural and Geotechnical Engineering, Sapienza University of Rome, Rome, Italy, alessandra.rosati@uniroma.1.it

Domenico Gaudio
Department of Engineering, University of Cambridge, UK, Trumpington Street, Cambridge, UK

Claudio Giulio di Prisco
Department of Civil and Environmental Engineering, Polytechnic University of Milan, Milan

ABSTRACT: Caisson foundations are usually subject to combined loading both under working conditions and during exceptional events such as earthquakes and tsunamis, during which the foundation experiences states of stress close to its bearing capacity. In this paper, failure envelopes of rigid and massive cylindrical caisson foundations are investigated via a set of parametric 3D push-over Finite Element (FE) numerical analyses. In particular, different (i) initial loading factors χ, (ii) caisson embedment ratios H/D and (iii) drainage conditions have been accounted for. The soil-caisson foundation interaction failure domains, defined in the N-Q-M generalized load space, have been derived and critically discussed providing a comparison with similar results available in the literature. Numerical results are also validated against both upper and lower bound Limit Analysis (LA) solutions. The numerical results presented in this work can be analytically interpreted and used (i) for the evaluation of the performance of a caisson under static conditions with respect to both serviceability and ultimate limit states and (ii) to develop an elastic-plastic macro element model for caisson foundations.

RÉSUMÉ : Les fondations sur caissons sont habituellement sollicitées par des chargements combinés le long de leur exploitation et pendant les situations de projet exceptionnelles (séismes, tsunamis, etc.), les états de contrainte ainsi associés sont proches de leur capacité portante. Dans cet article, les enveloppes de rupture des caissons de fondations massifs, rigides et cylindriques, sollicités par chargement combinés (N-Q-M), sont analysées numériquement utilise à l'aide d'un jeu d'analyses push-over 3D aux éléments finis (FE). En effet, plusieurs (i) facteur de chargement χ, (ii) rapport d'encastrement H/D et (iii) conditions de drainage sont considérés. Les domaines de rupture de l'ensemble sol-fondation, définis dans l'espace N-M-Q, ont été validés et discutés de manière critique grâce à une comparaison avec les résultats d'expériences similaires issus de la littérature scientifique. Les résultats acquis sont aussi validés par les solutions obtenues par les analyses des limites supérieures et inférieures (LA). Les résultats présentés pourront être employées, dans le cas d'une fondation sur caissons, pour, d'une part, évaluer les performances d'une fondation sur caissons dans des conditions statiques par rapport aux états limites de services et ultimes, et d'autre part, développer un modèle élasto-plastique en macro-élément.

KEYWORDS: Caisson foundation, combined loading, bearing strength surface, failure mechanism, 3D numerical analysis

1 INTRODUCTION

Caissons are embedded foundations often employed for critical onshore infrastructures, such as long-span bridges and viaducts, usually subject to combined loading both under working conditions and during exceptional events, such as earthquakes. Caissons are generally either cylindrical or cuboid in shape and characterised by both large masses and stiffnesses. Their behaviour under ultimate conditions strongly differs from that of shallow and pile foundations since the contributions to bearing capacity of the caisson base and shaft are comparable. Due to their considerable dimensions, failure mechanisms, involving large surrounding soil volumes, lead to high both axial and lateral loading capacities.

Following a limit state approach, a foundation must be designed to provide an adequate factor of safety under the load combinations expected during its service life. The classic approach to foundation design requires the factor of safety to be evaluated as the ratio between the limit (N_{lim}) and the expected (N) vertical load, the former usually computed, under general loading conditions, by employing the classical solutions proposed by Froelich (1936) and Brinch Hansen (1970), where empirical coefficients are introduced to take both load inclination and eccentricity into account. A different approach is related to the use of interaction diagrams (IDs), three-dimensional envelopes defined in the N-Q-M space, where Q and M stand for horizontal force and overturning moment. The use of failure envelopes allows the factor of safety to be defined as either the minimum distance of the current N-Q-M combination from the envelope, or the distance evaluated along a given loading path.

Most of the studies available in the literature, conducted by means of both experimental and numerical approaches, regard shallow footings (Butterfield and Gottardi, 1994; Gouvernec and Randolph, 2003, Pisanò *et al*., 2014), solid and skirted embedded foundations for offshore structures (Yun and Bransby, 2007; Bransby and Yun, 2009), spudcan footing employed for offshore jack-up units (Martin, 1994) and only a few regard cuboid shaped massive onshore caissons (Gerolymos *et al*., 2015; Zafeirakos and Gerolymos, 2016).

In this paper the ultimate response of massive cylindrical caisson foundations under combined N-Q-M loads is investigated by means of a series of 3D FE non-linear static analyses carried out in terms of effective stresses for both undrained and drained conditions to properly take the two-phase nature of the foundation soil into account. Three typical embedment ratio values are considered (H/D = 0.5, 1, 2, being H the embedment depth and D the diameter) while the foundation soil is assumed to consist of an alluvial deposit, which is a recurring condition for onshore structures. To better understand the factors affecting dimensions and shape of failure envelopes, the results of a parametric study are here discussed, where foundation geometry,

initial stress and drainage conditions have been varied. The analytical description of the numerical results, consisting in relationships for the IDs in *N*-*Q*-*M*/*D* load space and for non-dimensional generalized load-displacement curves relative to both undrained and drained condition, here omitted for the sake of brevity, is presented in Rosati *et al*., 2020. Such expressions can provide a useful tool for evaluating the performance of a caisson foundation under static conditions with respect to both serviceability and ultimate limit states. The results of this study can also be used to develop an elastic-plastic macro-element model for massive caissons.

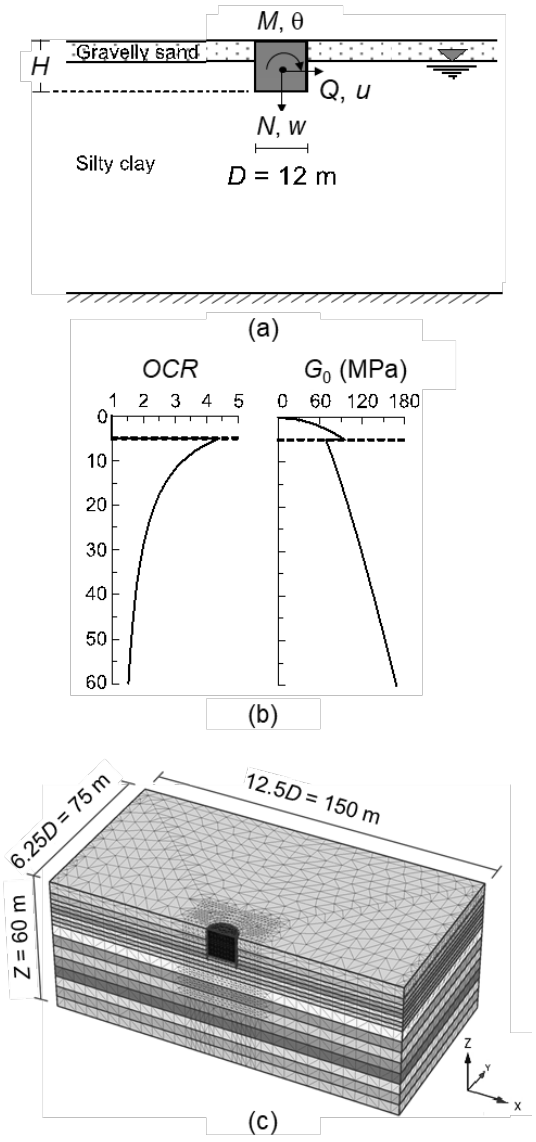

Figure 1. Problem definition: (a) schematic layout; (b) *OCR* and G_0 profiles assumed in the analyses; (c) 3D view of the FE model. (modified from Gaudio and Rampello, 2019a)

2 PROBLEM LAYOUT AND NUMERICAL MODELLING

A sketch of the problem layout is illustrated in Figure 1. A cylindrical caisson of diameter $D = 12$ m and height H is embedded in an alluvial deposit consisting of a 5-meter-thick layer of gravelly sand and a 55-meter-thick layer of silty clay. Water table is located at the bottom of the coarse-grained layer: an initial hydrostatic pore water pressure regime is assumed. While D is kept constant over the parametric study, three embedment ratios $H/D = 0.5, 1, 2$ are considered. The load reference point (LRP), defined as the point where loads and displacements are referred to, unless differently specified, is chosen to be coincident with the caisson centroid and the sign convention adopted in the analyses is also illustrated in Figure 1a.

The silty clay underlying the layer of gravelly sand is assumed to be slightly overconsolidated due to a uniform erosion process. The profiles adopted in the analyses for the overconsolidation ratio *OCR* and the small-strain shear modulus G_0 are plotted in Figure 1b. G_0 increases with depth according to the empirical relationship proposed by Hardin and Richart (1963) for the gravelly sand and by Rampello *et al*. (1995) for the silty clay. The earth pressure coefficient at rest is evaluated by using the relationship proposed by Mayne and Kulhawy (1982). A linear elastic-perfectly plastic behaviour is assumed for the foundation soils with a Mohr-Coulomb failure criterion. The soil properties assumed in the analyses are listed in Table 1, where γ is the unit weight, ν the Poisson's ratio, G/G_0 the ratio between the current and the small-strain shear modulus, c' the cohesion, φ' the internal friction and ψ the dilatancy angles.

Table 1. Properties of foundation soils

Soil	γ (kN/m^3)	ν	G/G_0	c' (kPa)	φ' (°)	ψ(°)
Gravelly sand	20	0.2	0.50	0	30	0
Silty clay	20	0.2	0.37	20	23	0

The numerical analyses have been carried out using the FE code Plaxis 3D AE (Brinkgreve, 2013). The 3D FE mesh used in case of $H/D = 0.5$ and 1 (Figure 1c) consists of 95500 10-node tetrahedral elements with 4 Gaussian points, while in case of $H/D = 2$, the depth of the model has been doubled, leading to a 115-meter-thick layer of silty clay and a mesh of approximately 188000 elements. Owing to the problem symmetry with respect to the *x*-axis only half domain has been modelled. Horizontal displacements on vertical boundaries, as well as horizontal and vertical displacements at the model base, are not allowed. In the analyses, the caisson is always wished in place, ignoring the simulation of the construction process. A linear elastic behaviour is assumed for the caisson with a Young's modulus $E_c = 30$ GPa and a Poisson's ratio $\nu = 0.15$; the unit weight of reinforced concrete is assumed equal to $\gamma_c = 25$ kN/m^3. At the soil-caisson contact, to simulate relative sliding, purely attritive interface elements, obeying the Mohr-Coulomb failure criterion, are inserted, with a friction angle $\delta = \tan^{-1}[2/3 \tan\varphi']$. More details about numerical modelling are given in Gaudio and Rampello (2019b).

3 ANALYSES AND RESULTS

In order to investigate the bearing capacity under a general load combination, about 370 load-controlled push-over numerical analyses have been performed. They consist of the following calculation phases: (i) initialisation of the effective stress state; (ii) drained caisson activation; (iii) drained application of a vertical load N atop the caisson; (iv) either drained or undrained progressive load application up to failure by keeping constant ratio $\alpha_T = M_T/Q_T$, where Q_T and M_T are the horizontal force and overturning moment atop the caisson ("T" standing for "top"), respectively. Values of both Q_T and M_T are then transposed into equivalent forces and moments referred to the foundation centroid, chosen as LRP: $Q_G = Q_T$ and $M_G = M_T + Q_T \cdot H/2 = (\alpha_T + H/2) \cdot Q_T = \alpha_G \cdot Q_G$ (subscript "G" referring to the caisson centroid). Ratio α_G represents the lever arm of load component Q_G measured from the caisson centroid. Drainage conditions have been varied during phase (iv) when both horizontal forces and overturning moments are applied,

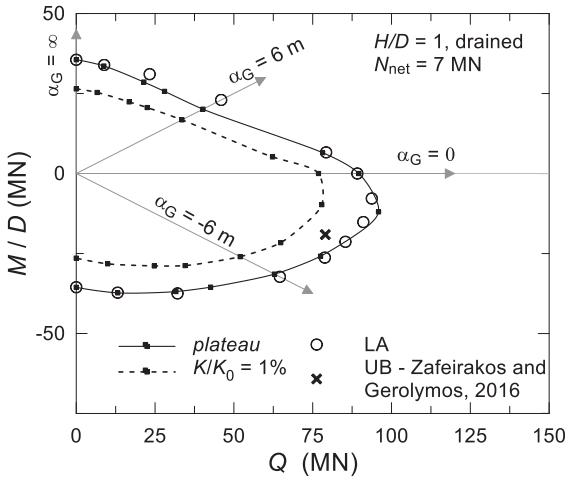

Figure 2. Different criteria for defining ultimate loads: IDs for $H/D = 1$ under drained conditions. Comparison to LA results.

assuming that such components are associated with transient events occurring under undrained conditions.

For $H/D = 1$ and drained conditions the section of ID in the Q-M/D plane, corresponding to $N_{net} = 7$ MN is represented in Figure 2 (solid line). Owing to its symmetry with respect to the origin of the plane, only half of the envelope is represented. Net vertical load, N_{net}, denotes the net disturbance $N_{net} = N + W_c - \sigma_{v0(z=H)} \cdot A_c$, where N is referred to the top of the caisson, W_c and A_c are the caisson weight and cross-section area, respectively, and σ_{v0} is the lithostatic total vertical stress acting at the embedment depth $z = H$. It is worth pointing out that when a zero vertical load is applied atop the caisson the value of N_{net} is different from zero due to the different values of γ for soil and caisson (for $H/D = 1$, in Figure 2, $N = 0$ leads to $N_{net} \approx 7$ MN). For the sake of clarity, some of the radial loading paths imposed during the calculation phase (iv), corresponding to different values of α_G, are also represented in the figure (arrows). Each point of ID corresponds to the attainment of the *plateau* of the push-over curve represented in the non-dimensional generalised force-displacement plane $|\bar{F}| - |\bar{u}|$, where:

$$|\bar{F}| = \sqrt{\left(\frac{Q}{N_{lim,net}}\right)^2 + \left(\frac{M}{D \cdot N_{lim,net}}\right)^2} = \sqrt{\left(\frac{Q}{N_{lim,net}}\right)^2 + \left(\frac{\alpha_G Q}{D \cdot N_{lim,net}}\right)^2} \quad (1)$$

$$|\bar{u}| = \sqrt{\left(\frac{u}{D}\right)^2 + (\theta)^2}$$

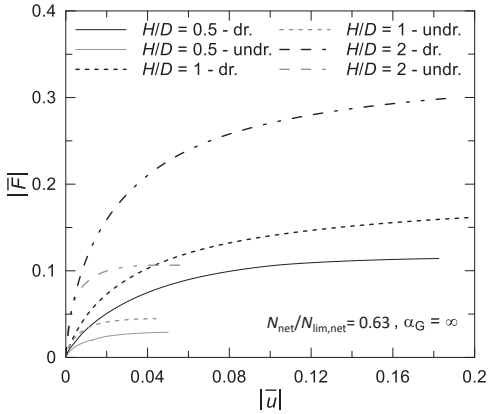

Figure 3. Non-dimensional generalised push-over curves.

where $N_{lim,net}$ is the ultimate value of the centered vertical load under drained conditions, numerically determined for any H/D value, u and θ are caisson horizontal displacement and rotation, respectively. From the analysis of the numerical curves we derive that the collapse of the soil-foundation system under a general N-Q-M load combination (*plateau* of the push-over curves) is attained for values of displacements varying in a wide range: from centimetres to metres, depending on the (i) loading path (α_G), (ii) embedment ratio (H/D), (iii) vertical load (N_{net}) and (iv) drainage conditions. The highest values of displacements are attained under drained conditions for the deepest caissons ($H/D = 1$, 2) subject to high vertical loads. Indeed, under such conditions punching rather than general failure mechanisms develop and the associated accumulated generalised displacements are definitely incompatible with the superstructure performance. In Figure 3 the generalised force-displacement curves obtained for the three caissons subject to the same initial vertical loading ratio ($N_{net}/N_{lim,net} = 0.63$) and load path ($\alpha_G = \infty$) under both drainage conditions are compared: the drained curves relative to the deepest caissons ($H/D = 1$ and 2) do not attain a well-defined *plateau* despite the high values of $|\bar{u}|$. Therefore, as suggested by Gerolymos *et al*. (2015), a different criterion to define the ultimate condition is adopted here, such as the attainment of a tangent stiffness in the push-over curve equal to 1% of the initial one ($K_{tan}/K_0 = 1\%$). Such a condition leads to the evaluation of limit loads corresponding to computed displacements much smaller than that referred to the *plateau* of the push-over curves. However, as it is apparent in Figure 2, IDs obtained by using the two different above criteria seem to be homothetic.

In Figure 2, the results of the FE push-over analyses are also compared with those provided by Limit Analysis using the code OPTUM G3, in which LA calculations are combined with FE method (Sloan, 2013). In LA calculations, to obtain results comparable to those of the FE analyses in which the flow rule is

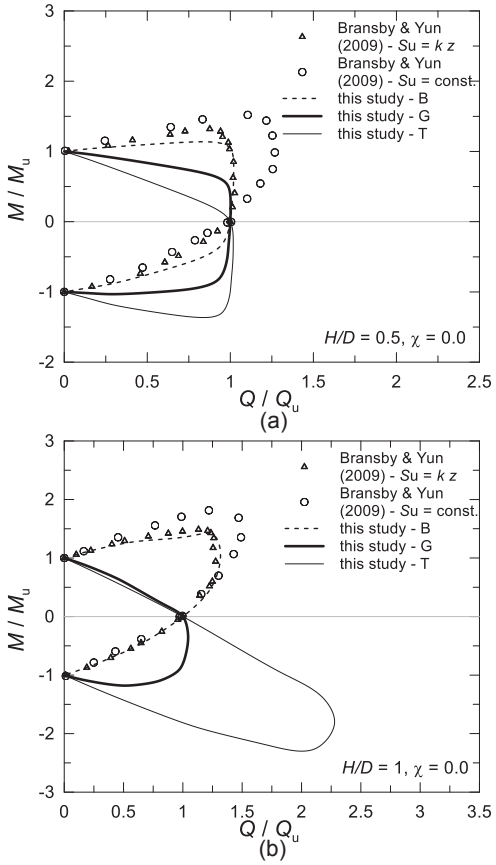

Figure 4. Influence of LRP: IDs obtained for caissons with $\chi = 0$ and undrained conditions, for (a) $H/D = 0.5$ and (b) 1.

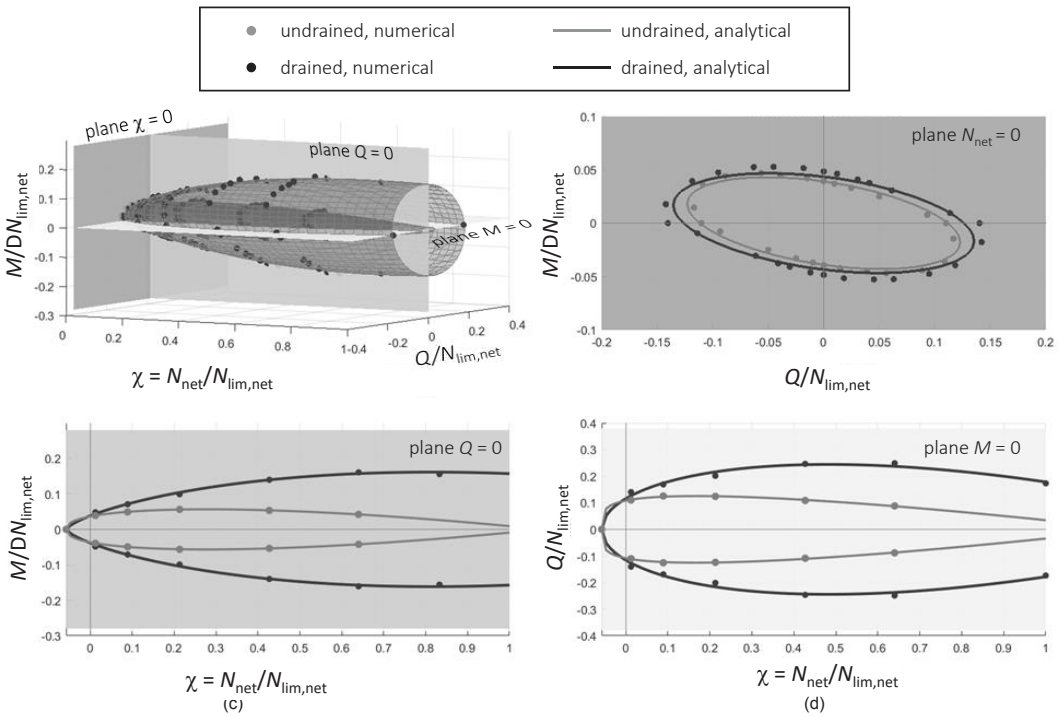

Figure 5. IDs for $H/D = 1$ under undrained and drained conditions: (a) $N_{net}/N_{lim,net}$ -$Q/N_{lim,net}$ -$M/[DN_{lim,net}]$ space, (b) $N_{net} = 0$ plane, (c) $Q = 0$ plane, (d) $M/D = 0$ plane.

non-associated ($\psi = 0$), strength parameters are reduced as was proposed by Davis (1968). For each loading path the agreement observed between the two calculation approaches can be deemed more than satisfactory. A comparison between the computed ID and the upper-bound (UB) solution provided by Zafeirakos and Gerolymos (2016) for the mechanism of pure sliding of a cuboid-shaped caisson in the absence of any vertical load atop the caisson is also presented. A fair agreement is observed and the small differences are likely to be due to the different geometry of the caisson assumed in this study (cylindrical).

4 PARAMETRIC STUDY

In this section the results of a parametric study, in which (i) the initial loading factor $\chi = 1/F_{Sv}$, (ii) caisson embedment ratio (H/D), and (iii) drainage conditions have been varied, are presented, where $F_{Sv} = N_{lim,net}/N_{net}$ denotes the safety factor in the case of a centred vertical load under drained conditions. The vertical load applied in the calculation phase (iii), described in Section 3, has been chosen to impose the same value of χ, so that the same shear strength is mobilised in the foundation soils of each caisson before progressively increasing the horizontal force and the overturning moment. Five values of χ have been chosen ($\chi = 0$, 0.09, 0.21, 0.42, 0.63), these resulting in $F_{Sv} = \infty$, 11, 4.7, 2.4, 1.6. Furthermore, the influence of the choice of LRP on IDs shape is first discussed in the following.

4.1 *Influence of LRP location*

Bearing in mind that LRP can be chosen arbitrarily, the most frequently adopted location is the top, the centroid and the base of the foundation. The effect of LRP location is presented in Figure 4 for IDs computed under undrained conditions for caissons with embedment ratios $H/D = 0.5$ and 1.0 and without any vertical load atop the caisson ($\chi = 0$). Three different LRPs are considered: base (B), centroid (G) and top of the caissons (T). In order to focus on the IDs shape, they have been represented in non-dimensional plane Q/Q_u-M/M_u, where Q_u and M_u denote respectively the values of Q and M bringing the soil-caisson systems to collapse when the other component is zero: $Q_u = Q_{(M = 0)}$ and $M_u = M_{(Q = 0)}$.

For both values of H/D IDs referred to the base are compared with the results provided by Bransby and Yun (2009) for massive caissons embedded in a homogeneous layer of clay characterised by (i) constant (circles) and (ii) linearly increasing (triangles) undrained shear strength s_u. Although the analyses of Bransby and Yun (2009) have been performed in terms of total stresses, their results for the case (ii) are in very good agreement with the IDs computed in this study: this can be attributed to the occurrence that the soil shear strength increases with depth in this study, too.

By comparing the IDs computed adopting different locations of LRP, we derive that ID relative to the deepest caisson (line T in Figure 4b) is characterized by a more "stretched" shape with Q and M components acting in opposite directions (IV quadrant); indeed, the overturning moment counterbalances the moment produced by the horizontal force applied at the caisson's head. This is the reason why the eccentricity becomes more and more pronounced with H/D. The corresponding domains referred to G are substantially more symmetric with respect to the axes. For the shallower caisson ($H/D = 0.5$, Figure 4a) the envelope is almost symmetric, as well as perpendicular to the axes: this is due to the decoupling between rotational and horizontal degrees of freedom. Indeed, for a caisson with $H/D = 0.5$ only subject to M ($\alpha_G = \infty$), the computed failure mechanism consists of an almost pure clockwise rotation closely around the centre of gravity G; similarly, when subject to Q ($\alpha_G = 0$), the caisson undergoes a pure sliding mechanism. Such a condition of decoupling fails for higher values of the embedment ratio (Figure 4a) because the lever arm of the resultant force (external + soil reaction) transferred to the caisson centroid increases with increasing embedment H. Hence, for high values of H/D the pure sliding mechanism corresponds to a horizontal force applied at a point deeper than G, at a depth $z \approx 2/3\ H$.

4.2 *Influence of the initial loading factor*

To appreciate the influence of initial loading factor χ on the size of IDs, the authors have plotted in Figure 5a in N_{net}-Q-M/D space normalised with respect to $N_{lim,net}$, IDs obtained for $H/D = 1$ under both undrained and drained conditions. The numerical results (black and grey full circles) have been also analytically interpolated (black and grey solid lines) (Rosati *et al*., 2020). The analytical corresponding expressions of the curves are here omitted for the sake of brevity. For the sake of clarity, cross sections of IDs on $N_{net} = 0$, $Q = 0$, $M = 0$ planes are represented in Figure 5b, c, d, respectively for undrained conditions, due to the progressive change in the failure mechanisms, becoming deeper and more asymmetric, ID first expands and then shrinks for increasing χ values. Specifically, due to the mobilisation of shear strength in a larger volume of the soil surrounding the caisson, particularly beneath the foundation, as mechanisms deepen, bearing capacity increases. However, starting from a threshold value of χ, reduction in bearing capacity, caused by asymmetry in the mechanisms, prevails and then envelopes start contracting. As far as the drained conditions are concerned, after an initial expansion, ID seems to maintain an "open" shape when approaching the limit value $\chi = 1$ ($N_{net} = N_{lim,net}$), this suggesting a non-convex shape for ID when $N_{net} > N_{lim,net}$. It is worth mentioning that IDs also extend to the portion of the load space where $N_{net} < 0$ (traction) due to the contribution of the shaft resistance to bearing capacity.

For caissons characterized by $H/D = 1$ and 2, the influence of χ on the shape of IDs in $Q/Q_u - M/M_u$ plane appears not to be remarkable: the non-dimensional IDs almost overlap (Figure 7). In contrast, for the shallowest caisson ($H/D = 0.5$) a radical change in shape is observed passing from $\chi < 0.1$ to $\chi > 0.1$, but the relative IDs are not plotted in Figure 7 for the sake of graphical clarity.

4.3 *Influence of the embedment ratio*

Influence of the embedment ratio on both size and shape of IDs is shown in Figure 6. For both drainage conditions and a given value of χ, as was expected, due to the progressive deepening of the failure mechanism (Figure 6a for $\chi = 0.09$ and undrained conditions), the size of IDs related to the deeper caissons is always larger. As far as the shape is concerned, H/D seems to cause a significant change when $\chi \leq 0.21$: as H/D increases (black lines in Figure 6b): the envelope eccentricity progressively increases in the IV quadrant of the non-dimensional plane. For high values of the vertical load (grey lines in Figure 6b) the influence of H/D on the IDs shape vanishes.

4.4 *Influence of drainage conditions*

For assigned values of both χ and H/D, under undrained conditions, smaller failure envelopes with respect to those computed in case of drained conditions (Figure 5) are obtained. As is well known, this is a consequence of the local arising of excess pore water pressure within the soil domain associated with both compression loading and inhibited drainage. However, drainage conditions do not affect the shape of the failure envelopes in terms of non-dimensional IDs in plane Q/Q_u – M/M_u. This is evident in Figure 7, where IDs under undrained and drained conditions for $H/D = 1$ and $\chi = 0.09$ and 0.42 are plotted.

5 FINAL REMARKS

Rigid and massive caisson foundations are typically subject to combined loading under working and ultimate state conditions, in which the foundation experiences states of stress close to its bearing capacity. For this reason, in the design of caisson foundations, the interaction domains (IDs) may be a useful tool to assess their safety against limit states. In this paper, the bearing capacity of massive cylindrical onshore caisson foundations subject to combined loading has been investigated by means of an extensive set of 3D elastic-perfectly plastic FE numerical analyses, in order to understand the factors that mainly affect the size and the shape of IDs in Q-M plane. Attention has been focused on the influence of the initial loading factor (χ), the caisson embedment ratio (H/D) and the drainage conditions. It has been shown that: (i) as χ increases the envelopes first undergo an expansion and thereafter a contraction, (ii) the influence of χ on the shape is remarkable for small values of H/D only. Similarly, the embedment ratio affects the shape of the envelopes only for small values of χ and, as H/D increases, an expansion of the envelope is observed. The drainage conditions appear to have an influence on the envelopes size only: the envelopes obtained under undrained conditions are always smaller than the corresponding ones computed under drained conditions, while their shape does not vary significantly. The influence of the choice of the load reference point has also been discussed. The centroid of the caisson has been considered the most suitable choice, as this strongly simplifies the shape of ID,

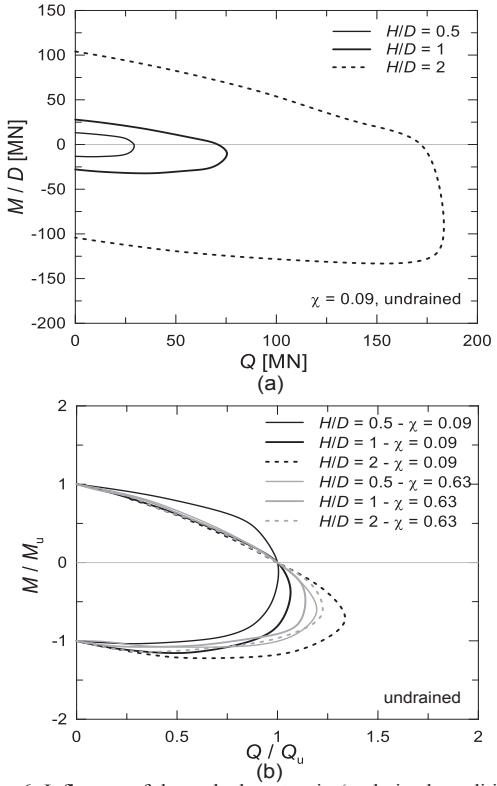

Figure 6. Influence of the embedment ratio (undrained conditions): (a) $\chi = 0.09$; (b) $\chi = 0.09$ and 0.63.

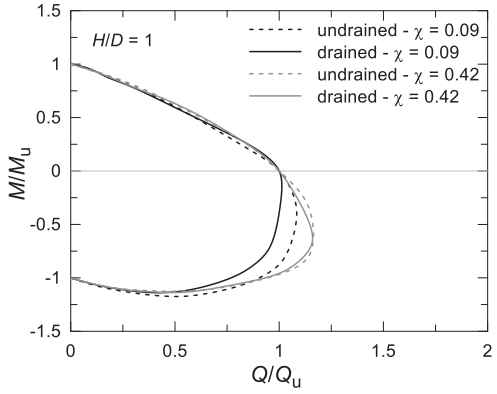

Figure 7. Influence of drainage conditions: IDs obtained for $H/D = 1$ and $\chi = 0.09$ and 0.42.

leading to the decoupling between rotational and translational degrees of freedom, especially for low embedment ratios.

The IDs provided by the numerical analyses represented in *N*-*Q*-*M*/*D* load space present a "rugby ball" shape as those obtained in previous works for shallow footings. However, in contrast with what observed in case of shallow foundations, soil-caisson strength under *Q*-*M* combinations is different from zero when the vertical load is equal to either zero or to its limit value ($N_{lim,net}$): the latter aspect becomes more and more evident as *H*/*D* increases and under drained conditions.

The numerical results can be analytically interpolated to derive a mathematical expression for three-dimensional IDs in *N*-*Q*-*M*/*D* space for both undrained and drained conditions. The interaction domain can be used to evaluate the safety factor at the design stage of a caisson foundation under static conditions, as well as to develop a macro-element models based, for instance, on the theory of elastic-plasticity.

From an engineering point of view, to compute foundation generalized displacements and perform a simplified displacement based design, from a suitable analysis of the numerical results analytical expressions describing non-dimensional generalised load-displacement curves can also be derived and, once the same shape is assumed for yielding and failure envelopes (isotropic hardening), these expressions can be also used to compute the IDs corresponding to an assigned value of the generalised displacement $|\bar{u}|$. This use of the numerical results is presented in Rosati *et al*., 2020.

6 REFERENCES

Bransby, M.F., Yun, C.J., 2009. The undrained capacity of skirted strip foundations under combined loadings. *Géotechnique*, 59(2), 115-125.

Brinch Hansen, J., 1970. A revised and extended formula for bearing capacity. *Bulletin No. 28*, 5-11.

Brinkgreve, R.B.J., Engin, E., Swolfs, W. M., 2013. *PLAXIS 3D*. Reference Manual.

Butterfield, R., Gottardi, G., 1994. A complete three-dimensional failure envelope for shallow footings on sand. *Géotechnique*, 44(1), 181-184.

Davis, E. H., 1968. Theories of plasticity and the failure of soil masses. In: *Selected Topics in Soil Mechanics*. Lee, I. K., Editor, Butterworth, London.

Froelich X., 1936. Beitrag fur Berechnung von Mastfundamenten. Ernest, Berlin.

Gaudio D., Rampello S., 2019a. A simplified procedure for the evaluation of the seismic performance of bridge piers on caisson foundations. In: *Proceedings of COMPDYN 2019*, Crete, Greece, 1946-1956.

Gaudio D., Rampello S., 2019b. The role of soil constitutive modelling on the assessment of seismic performance of caisson foundations. In: *Proceedings of the 7th International Conference on Geotechnical Earthquake Engineering*, Rome, Italy, 2574-2582.

Gouvernec, S., Randolph, M., 2003. Effect of strength non-homogeneity on the shape of the failure envelopes for combined loading of strip and circular foundations on clay. *Géotechnique,* 53(6), 575-586.

Gerolymos, N., Zafeirakos, A., Karapiperis, K., 2015. Generalized failure envelope for caisson foundations in cohesive soil: Static and dynamic loading. *Soil Dynamics and Earthquake Engineering*, 78, 154-174.

Hardin, B. O., Richart, F. E., 1963. Elastic wave velocities in granular soils. *Soil Mechanics and Foundation Division,* 89, 33-65.

Martin, C.M., 1994, Physical and numerical modelling of offshore foundations under combined loads. PhD Thesis, University of Oxford, Oxford.

Mayne, P. W., Kulhawy, F. H., 1982. K0 - OCR relationships in soil. *Journal of the Geotechnical Engineering Division,* 108(6), 851-872.

Pisanò, F., di Prisco, C. G., Lancellotta, R., 2014. Soil-foundation modelling in laterally loaded historical towers. *Géotechnique*, 64(1), 1-15.

Rampello, S., Viggiani, G., Silvestri, F., 1995. Panelist discussion: The dependence of G_0 on stress state and history in cohesive soils. In: I International Symposium on Pre-Failure Deformation Characteristics of Geomaterials, Sapporo, Balkema, 2, 1155-1160.

Rosati, A., Gaudio, D., di Prisco, C.G., Rampello, S., 2020. Use of interaction domains for caisson foundations. Submitted for publication to *Géotechnique*.

Sloan, S. W., 2013. Geotechnical stability analysis. *Géotechnique,* 63(7), 531-572.

Yun, G., Bransby, M.F., 2007 b. The horizontal-moment capacity of embedded foundations in undrained soil. *Canadian Geotechnical Journal,* 44(4), 409-424.

Zafeirakos, A., Gerolymos, N., 2016. Bearing strength surface for bridge caisson foundations in frictional soil under combined loading. *Acta Geotechnica,* 11(5), 1189-1208.